AUTHOR QUERY FORM

[ELSEVIER logo] **ELSEVIER**	**Journal:** EA	**Please e-mail or fax your responses and any corrections to:**
		E-mail: corrections.esch@elsevier.thomsondigital.com
	Article Number: 20046	**Fax:** +353 6170 9272

Dear Author,

Please check your proof carefully and mark all corrections at the appropriate place in the proof (e.g., by using on-screen annotation in the PDF file) or compile them in a separate list. Note: if you opt to annotate the file with software other than Adobe Reader then please also highlight the appropriate place in the PDF file. To ensure fast publication of your paper please return your corrections within 48 hours.

For correction or revision of any artwork, please consult http://www.elsevier.com/artworkinstructions.

Any queries or remarks that have arisen during the processing of your manuscript are listed below and highlighted by flags in the proof. Click on the 'Q' link to go to the location in the proof.

Location in article	Query / Remark: **click on the Q link to go** **Please insert your reply or correction at the corresponding line in the proof**
Q1 Q2	Please confirm that given names and surnames have been identified correctly. Please provide article titles for all references. Please check this box or indicate your approval if you have no corrections to make to the PDF file □

Thank you for your assistance.

Graphical Abstract

Electrochimica Acta xxx (2013) xxx–xxx
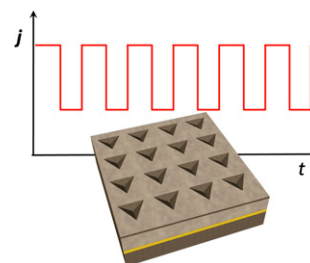
Tailoring the physical properties of electrodeposited CoNiReP alloys with large Re content by direct, pulse, and reverse pulse current techniques

S. Pané*, B. Özkale, K.M. Sivaraman, C. Ruiz-Camps, S. Suriñach, M.D. Baró, B.J. Nelson, J. Sort*, E. Pellicer**

Tailoring the physical properties of electrodeposited CoNiReP alloys with large Re content by direct, pulse, and reverse pulse current techniques

Q1 S. Pané [a,∗], B. Özkale [a], K.M. Sivaraman [a], C. Ruiz-Camps [b], S. Suriñach [b], M.D. Baró [b], B.J. Nelson [a], J. Sort [c,∗], E. Pellicer [b,∗∗]

[a] Institute of Robotics and Intelligent Systems (IRIS), ETH Zürich, CH-8092 Zürich, Switzerland
[b] Departament de Física, Facultat de Ciències, Universitat Autònoma de Barcelona, E-08193 Bellaterra, Spain
[c] Institució Catalana de Recerca i Estudis Avançats (ICREA) and Departament de Física, Universitat Autònoma de Barcelona, E-08193 Bellaterra, Spain

ARTICLE INFO

ABSTRACT

The composition, surface morphology and structure of CoNiReP alloy films with large Re content (up to 27 at%), obtained in a citrate-glycine based electrolyte have been studied as a function of the electrodeposition technique. Direct current (DC), pulse plating (PP) and reverse pulse plating (RPP) were considered with cathodic current densities from $-50\,\mathrm{mA\,cm^{-2}}$ to $-250\,\mathrm{mA\,cm^{-2}}$. The mechanical and magnetic properties have been analyzed and the data obtained has been correlated with composition and crystallographic structure. For values of j (DC), j_{on} (PP) and j_c (RPP) below $-100\,\mathrm{mA\,cm^{-2}}$, Co-rich, P-containing deposits are obtained. Beyond these current densities, both the quantities of Ni and Re increase simultaneously at the expense of Co and P, the latter virtually falling to zero. The highest Re percentage (25–27 at%) was achieved in both PP and RPP conditions at a cathodic pulse of $-250\,\mathrm{mA\,cm^{-2}}$. All the films were either entirely nanocrystalline in nature or partially amorphous. Hardness values as high as 9.2 GPa have been found in PP plated $Co_{64}Ni_{18}Re_{18}$ deposits. Besides the large hardness, the incorporation of Re in the films leads to high elastic recovery values. The magnetic character of the deposits ranges from soft to semi-hard ferromagnetic.

© 2013 Published by Elsevier Ltd.

1. Introduction

CoNiReP based alloys were extensively investigated during the 1990s for applications in perpendicular magnetic recording media. Osaka's group contributed significantly in this field by producing electroless-deposited continuous films and patterned nanostructures of CoNiReP [1–5]. These films were mostly Ni-rich, and only under specific conditions, did the Co content surpass that of Ni. For example, a series of CoNiReP alloys in which the Co content could be varied from 0 to 54 at% as a function of the $CoSO_4$ concentration in the bath were electroless-deposited from a malonate-based formulation at pH 9.6 [6]. Coercivity values as high as ∼1.3 kOe along the perpendicular-to-plane direction were achieved in 0.25 μm-thick $Co_{25.8}Ni_{57}Re_{5.8}P_{11.7}$ films [1]. Further structural analyses of some of the investigated films revealed a microstructure in which segregated Co-rich crystalline particles were dispersed within NiP-based, nonmagnetic, low-crystalline regions [3,5]. Encouraged by

the superior corrosion-resistant and diffusion barrier properties of NiP- and CoP-based alloys, Valova and co-workers resumed the efforts on the electroless deposition of these systems with the inclusion of refractory metals such as Re [7]. Co-rich films containing Re up to 16.5 at% and very low P (around 1 at%) with hexagonal close-packed (hcp) structure and $\langle 1\,0\,0\rangle$ texture were synthesized. Despite a thorough structural analysis of these systems and studies of their corrosion behaviour, their magnetic and mechanical properties received little consideration [7].

Compared to electroless deposition method, electrodeposition offers numerous advantages for the production of CoNiReP-based alloys. Co-rich alloys can be readily obtained by electrodeposition from neutral or slightly acidic baths by applying suitable current densities [8,9]. In contrast, electroless baths for this system are typically alkaline, which is often incompatible with most of the photoresists used in lithographically patterned substrates. Besides, the electroless formulations are often unstable with shorten bath lifetimes. Also, electroless deposition rates are relatively slow and deposits are limited in thickness and composition.

The electrodeposition of CoNiReP alloys has received little attention. Most of the literature is focused on electrodeposited binary and ternary alloys containing Re. For example, Naor et al. have recently produced binary NiRe alloys by electrodeposition

∗ Corresponding authors.
∗∗ Corresponding author. Tel.: +34 935811401.
E-mail addresses: vidalp@ethz.ch (S. Pané), jordi.sort@uab.cat (J. Sort), Eva.Pellicer@uab.cat (E. Pellicer).

Table 1
Composition of the electrolyte [9].

Species	Chemical	c (mol dm^{-3})
Metal salts	$CoSO_4 \cdot 7H_2O$	0.05
	$NiSO_4 \cdot 6H_2O$	0.03
	$NiCl_2 \cdot 6H_2O$	0.02
	$NaH_2PO_2 \cdot H_2O$	0.02
	NH_4ReO_4	0.01
Complexing agent	NH_2CH_2COOH (glycine)	0.05
	$C_6H_5Na_3O_7 \cdot 2H_2O$ (sodium citrate)	0.05
Electrolyte support	Na_2SO_4	0.5
Additives	$Ce_2(SO_4)_3$	2×10^{-5}
	Tergitol 08	2.5 (ml dm^{-3})
	L-Ascorbic acid	8.5×10^{-3}
	$C_7H_4NNaO_3S \cdot 2H_2O$ (sodium saccharinate)	0.005

Table 2
Parameters used for the production of CoNiReP films by DC, PP and RPP techniques.

DC

$-j/mA\,cm^{-2}$	t_{dep}/s
50	176
75	117
100	87
250	–

PP

$-j_c/mA\,cm^{-2}$	t_{on}/ms	t_{off}/ms
50	0.1	0.9
75		
100		
250		

RPP

$-j_c/mA\,cm^{-2}$	t_c/ms	$j_a/mA\,cm^{-2}$	t_a/ms
50	1	25	1
75		37.5	
100		50	
250		125	

encouraged by the excellent mechanical properties of Re metal [10]. Rhenium possesses a high melting point, large hardness and Young's modulus, low friction coefficient, high tensile strength and creep rupture strength [11]. In our previous work, Co-rich CoNiReP alloys were electrodeposited by direct current (DC) and reverse pulse plating (RPP) techniques within the current densities range from -10 to $-50\,mA\,cm^{-2}$ in a newly designed bath formulation [9]. The maximum amount of Re that could be incorporated into the deposits was 11 at% under RPP conditions using cathodic pulses of $-10\,mA\,cm^{-2}$ and anodic pulses of $+5\,mA\,cm^{-2}$. However, in this particular case the resulting films had a higher Ni content than that of Co (i.e., $Ni_{43}Co_{32}Re_{11}P_{13}$) and were non-magnetic. Conversely, ferromagnetic Co-based films were obtained in all other cases regardless of the technique (DC and RPP) and applied current density, but with lower Re content (between 7 and 10.5 at%). Increasing the amount of Re in the alloy could provide additional versatility to the material (e.g. mechanical stability at high temperatures or improved wear resistance and elastic recovery).

The goal of the present study is to explore the production of CoNiReP alloys by pulse plating (PP) and RPP techniques while applying peak pulse current densities in the range from -50 to $-250\,mA\,cm^{-2}$ in order to favour Re incorporation. The previously developed electrolyte formulation is used [9]. For the sake of comparison, DC films are also deposited, although in this case the deposits tend to detach from the substrate for current densities beyond $-100\,mA\,cm^{-2}$. Because of forced nucleation during each new cathodic pulse and the existence of both adsorption/desorption and crystallization events, deposits featuring a wider range of compositions and microstructures are expected for PP and RPP techniques. Not less important, the problems of deposit adhesion encountered in DC can be circumvented. By virtue of the advantages offered by PP and RPP over DC plating and by the selected window of cathodic pulse current densities, a large tunability in alloy composition (in particular, higher Re contents) and, consequently, in their microstructure, is achieved. The mechanical and magnetic properties of the electrodeposited films are studied in detail and correlated with composition and microstructure.

2. Experimental

The electrodeposition was performed in a thermostatized one-compartment three-electrode cell filled with 100 ml of solution. The electrolyte formulation is given in Table 1. The formulation is essentially based on a Watt's type bath and each component exhibits crucial role in the deposition. Sulphates were used as the main source of nickel and cobalt ions since sulphates influence minimally the electrocrystallization process. Chlorides were used for improving bath conductivity and for depolarizing the nickel anode.

The pH was adjusted to 4.5. A double junction Ag|AgCl reference electrode was used with 3 mol dm^{-3} KCl inner solution and an outer solution made of 1 mol dm^{-3} Na$_2$SO$_4$. All potentials are referred to this electrode. A nickel sheet acted as the counter electrode. An inert atmosphere was maintained inside the electrochemical cell by a blanket of nitrogen gas on top of the solution. The level of electrolyte in the cell and the pH of the bath were checked at the beginning and at the end of each deposition. The required acidity was maintained using NaOH and H$_2$SO$_4$. The working temperature was 55 °C. Deposition was conducted under gentle stirring (500 rpm) to ensure homogeneous composition throughout deposit thickness.

The working electrode consisted of 5 mm × 6 mm silicon chips (crystal orientation 100), on top of which a titanium adhesion layer of 50 nm and a gold seed-layer of 500 nm had been successively deposited through e-beam evaporation. Before being used for the electrochemical experiments (cyclic voltammetry and electrodeposition), the gold surface was degreased by first dipping it in acetone followed by iso-propanol and finally water. The three electrodes were connected to a Gamry Reference 3000 potentiostat/galvanostat which were controlled by the Gamry Framework software during DC electrodeposition and by the Gamry VFP-600 software during PP and RPP depositions.

Current densities in the range from $-50\,mA\,cm^{-2}$ to $-250\,mA\,cm^{-2}$ were applied in DC deposition and during the cathodic pulses in PP and RPP depositions (Table 2). For PP electrodeposition the on-time (t_{on}) and off-time (t_{off}) pulses were 0.1 and 0.9 ms (duty cycle, $\gamma' = 0.1$) [12]. In RPP depositions the cathodic pulse duration was set at $t_c = 1$ ms; the anodic pulse current density (j_a) was $j_a = |j_c|/2$, with a pulse duration of $t_a = 1$ ms (duty cycle, $\gamma' = 0.5$). The charge density was kept at 8.8 C cm^{-2} for all depositions.

The surface morphology of the deposits was observed using a Zeiss Merlin scanning electron microscope (SEM). The chemical composition of the deposits was analyzed by energy dispersive X-ray spectroscopy (EDX) at different locations of the film to confirm uniformity. Two replicas per sample were measured. Complementary atomic absorption spectroscopy (AAS) analyses were in agreement with EDX data. The deposits were cross-sectioned by focused ion beam (FIB) to determine the thickness, which varied between 2 μm and 4 μm. X-ray diffraction (XRD) patterns were obtained with a Philips X'Pert diffractometer using the Cu Kα radiation in the 30–70° 2θ range (0.03° step size, 10 s holding time).
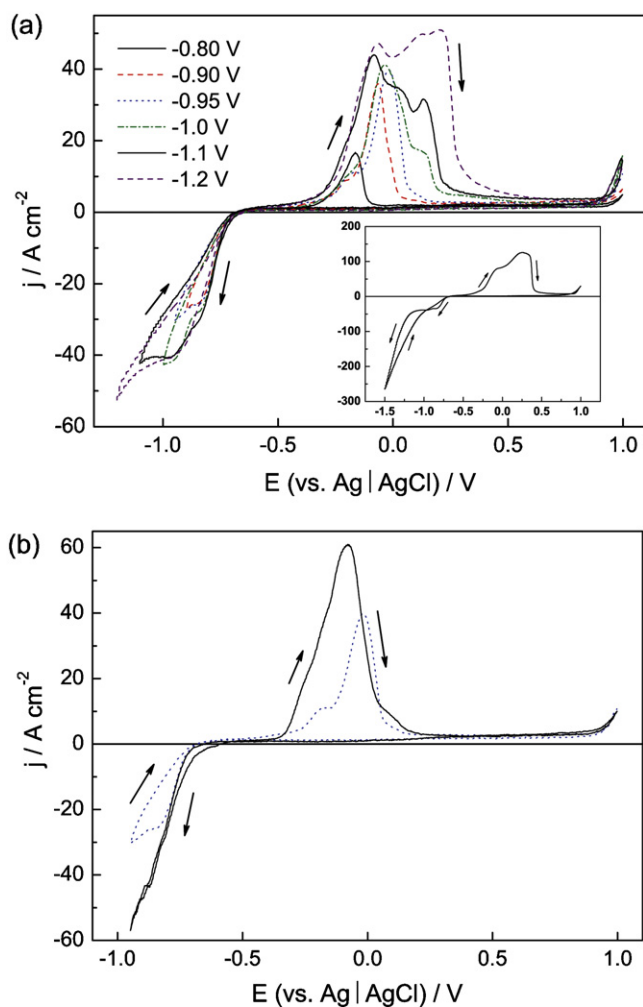
Fig. 1. CVs obtained on the Si/Ti/Au substrates, at a scan rate of 50 mV s⁻¹ for (a) cathodic limits −0.8, −0.9, −0.95, −1.0, −1.1, −1.2 and −1.5 V, quiescent conditions. The inset shows the CV for a cathodic limit of −1.5 V. (b) Cathodic limit of −0.95 V under quiescent (dashed line) and stirring (continuous line) conditions.

The crystallite size (or average coherent diffraction length, $\langle D \rangle$), microstrains (or atomic level deformations, $\langle \varepsilon^2 \rangle^{1/2}$) and stacking fault probability were evaluated by means of a full-pattern fitting procedure (Rietveld method) using the MAUD (Materials Analysis Using Diffraction) software [13,14].

The mechanical properties (hardness and reduced Young's modulus) were evaluated by nanoindentation using a Fischer Scripps Laboratories UMIS device equipped with a Berkovich pyramid-shaped diamond tip. The value of maximum applied force was chosen to be 20 mN to ensure that the maximum penetration depth during the tests was always kept below one tenth of the overall film thickness, which is considered as a necessary condition to avoid influence of the substrate on the measured mechanical properties of the film [15]. The thermal drift during nanoindentation was below 0.05 nm/s. Proper corrections for the contact area (calibrated with a fused quartz specimen), instrument compliance and initial penetration depth were applied. The results presented here represent the statistical average of a set of 100 indentations for each sample. The Berkovich hardness, H_B, and reduced Young's modulus, E_r, were derived from the load–displacement curves at the beginning of the unloading segment using the method of Oliver and Pharr [16]. Magnetic hysteresis loops, with an applied magnetic field up to 10 kOe, were measured at room temperature by vibrating sample magnetometry (Oxford Instruments), both along the in-plane
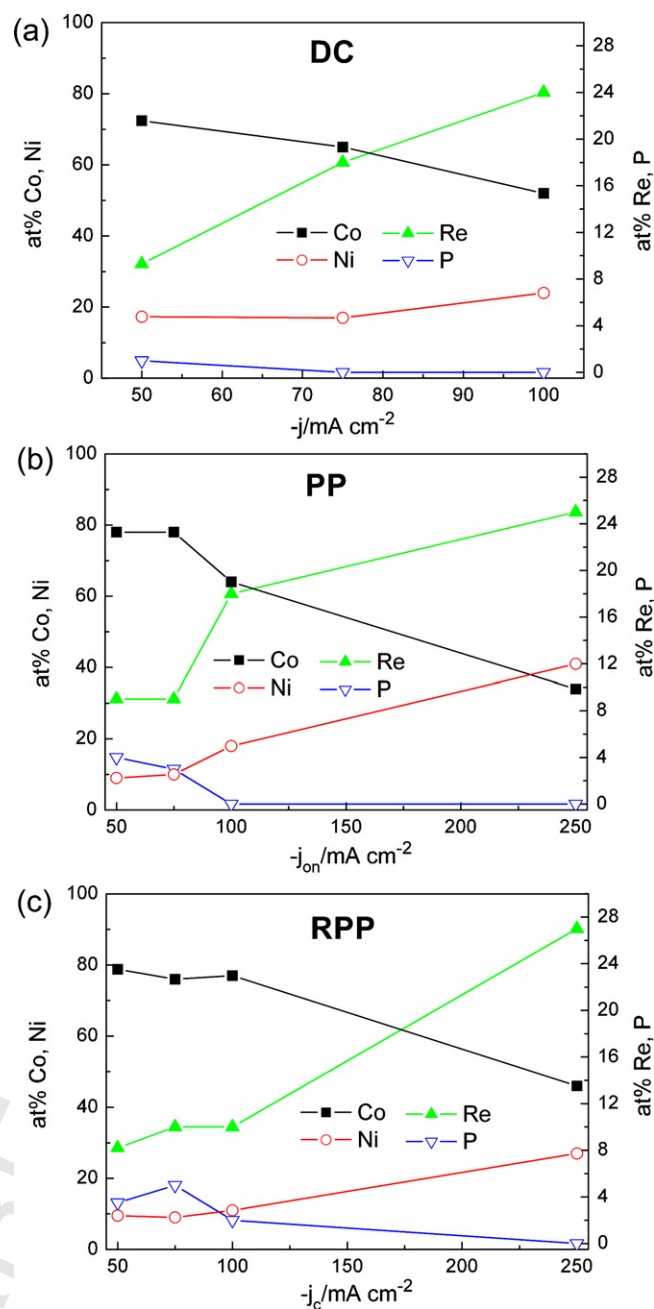
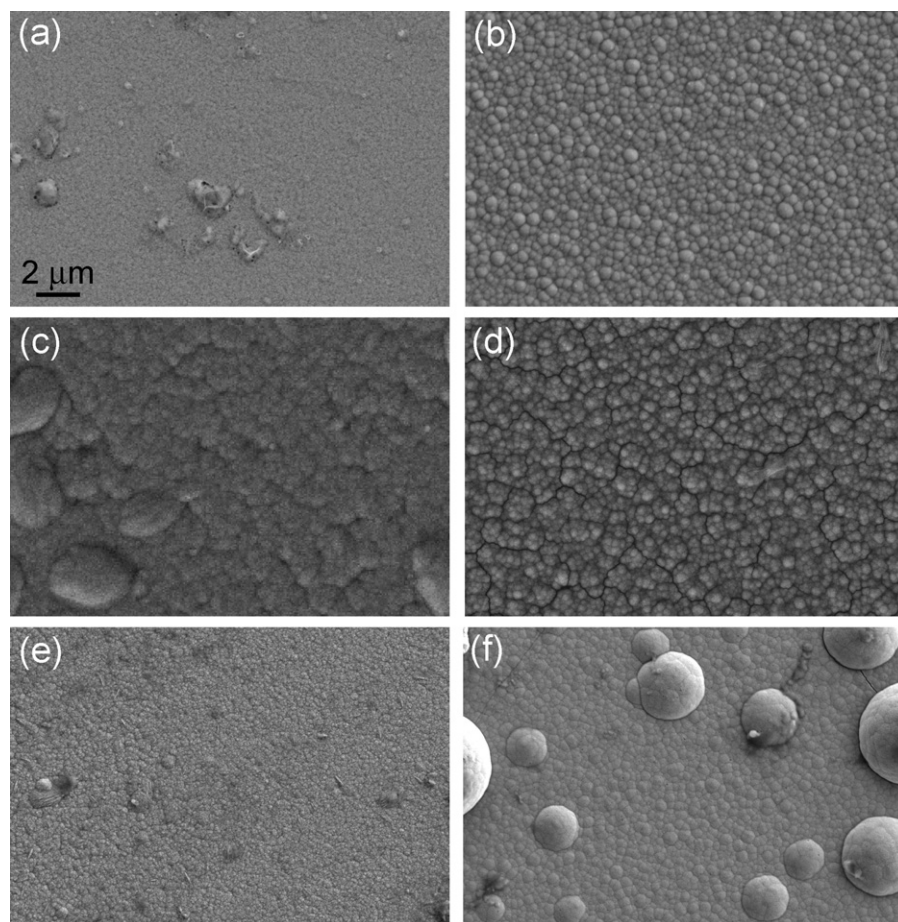**Fig. 2.** Composition of the CoNiReP layers obtained under (a) DC conditions as a function of the current density (j), (b) PP conditions as a function of the current density of the pulse (j_{on}), and (c) RPP conditions as a function of the current density of the cathodic pulse (j_c). Deviation is ±2 at.%.

and perpendicular-to-plane directions. Correction for the demagnetizing field was performed to accurately determine the magnetic properties [17–19].

3. Results and discussion

3.1. Cyclic voltammetry study

Fig. 1 shows the cyclic voltammetry (CV) curves obtained on Si/Ti/Au substrates (i.e., onto the upper Au seed-layer) from the electrolyte solution. In quiescent conditions the onset for deposition is around −0.7 V and a diffusion-controlled reduction peak is recorded in the negative scan (Fig. 1a). The oxidation response becomes progressively more complex as the cathodic limit is

Fig. 3. SEM images of the surface morphology of the CoNiReP layers obtained under (a) DC at $j = -75$ mA cm^{-2}, 2.4 μm; (b) DC at $j = -100$ mA cm^{-2}, 2.0 μm; (c) PP conditions at $j_{on} = -100$ mA cm^{-2}, 2.3 μm; (d) PP at $j_{on} = -250$ mA cm^{-2}, 2.6 μm; (e) RPP conditions at $j_c = -100$ mA cm^{-2}, 3.2 μm; and (f) RPP at $j_c = -250$ mA cm^{-2}; 4.0 μm. The scale is the same for all images.

enlarged, so that three partially overlapped peaks can be observed. Stirring of the solution supplies the electrode surface with fresh analyte, and the diffusion peak vanishes (Fig. 1b). Moreover, the oxidation response is simplified and a single oxidation peak is detected. Hence, stirring the solution is crucial to both ensure the formation of a homogeneous deposit and minimize pitting caused by the accumulation of hydrogen bubbles on the cathode surface, particularly at high current densities (high overpotentials).

3.2. Composition, morphology and structure of the deposits

The deposit characteristics can be largely tuned depending on the deposition technique. Fig. 2 shows the composition of the CoNiReP layers as a function of the deposition technique in the range of cathodic current densities between -50 and -250 mA cm^{-2} (up to -100 mA cm^{-2} for DC). Due to intense hydrogen evolution and consequent poor adherence, films could not be successfully deposited by DC at -250 mA cm^{-2}. In fact, one advantage of using pulse methods over DC electrodeposition is the possibility of applying large pulse current densities without film detachment [20]. In general, the Co content decreases as the value of j (for DC), j_{on} (for PP) and j_c (for RPP) becomes more negative. Simultaneously, the P content falls to zero and is virtually undetectable in deposits produced at current densities or pulses greater than -100 mA cm^{-2}. Conversely, the Ni and Re content increase in parallel, so that the samples grown at a current density of -100 mA cm^{-2} with DC or at a cathodic pulse of -250 mA cm^{-2} in PP and RPP conditions have the lowest Co/Ni ratio and the highest Re content

(around 25–27 at%). The films electrodeposited by PP conditions at $j_{on} = -50$ and -75 mA cm^{-2} have a very similar composition (i.e., they are Co-rich and the Re and P contents are of 9–10 at% and 4–3 at%, respectively) (Fig. 2b). The deposits feature much larger Ni and Re contents at $j_{on} = -100$ mA cm^{-2} and continue to increase up to -250 mA cm^{-2}, with virtually no P inclusion. This sharp change in composition is also observed in samples produced by RPP conditions (Fig. 2c). An increase in the Re content was also accompanied by a decrease in the P content even in the electroless deposition of NiReP alloys, both in alkaline citrate and acidic baths [21,22]. The same trend was observed in electroless deposited CoReP [23]. Variations in composition are more tepid under DC conditions (Fig. 2a). This could be due to the effect of the off-time pulse in PP and the anodic pulse in RPP on the mass transport during deposition [20].

Selected SEM images of DC, RPP and PP plated deposits are displayed in Fig. 3. An increase in the cathodic current density values apparently caused grain coarsening and promoted a rounded morphology of the grains. As a result, the deposit surface turned out to be much rougher. This is particularly evident in DC conditions, where a change from fine-grained deposits to larger, nodular-shape grains is observed with changing current density (cf. Fig. 3a and b). A transition from cotton-like to cauliflower-like deposit is observed under PP conditions (cf. Fig. 3c and d). Likewise, fine-grained, flat deposits evolve towards nodular-shaped grains under RPP conditions (cf. Fig. 3e and f). Since hydrogen evolution is exacerbated with current density, the formation of larger amounts of hydrogen bubbles onto the cathode could be partly responsible for the observed surface roughening. In order to further prove

Table 3
Summary of the microstructural parameters obtained from the Rietveld refinements of the XRD patterns: $I^{1/2}(1\,0\,0)/I^{1/2}(0\,0\,2)$ ratios (indicative of texture), average crystallite sizes ($\langle D \rangle$) and microstrains ($\langle \varepsilon^2 \rangle^{1/2}$).

Technique	$-j$, $-j_{on}$ or $-j_c$/mA cm^{-2}	$I^{1/2}(1\,0\,0)/I^{1/2}(0\,0\,2)$	$\langle D \rangle$/nm	$\langle \varepsilon^2 \rangle^{1/2}$
DC	50	12	19	4.5×10^{-4}
	75	0.5	20	1.4×10^{-3}
	100	–	–	–
PP	50	0	44	3.3×10^{-4}
	75	0.8	31	4.0×10^{-4}
	100	0.2	59	8.2×10^{-4}
	250	0.2	58	9.0×10^{-4}
RPP	50	4.8	49	1.0×10^{-4}
	75	0.1	65	2.7×10^{-4}
	100	0.2	47	3.4×10^{-4}
	250	–	10	4.1×10^{-3}

this effect, deposits were produced by PP at a cathodic current density of -500 mA cm^{-2}. Under these conditions, much rougher, cauliflower-like deposits with large nodular grains were observed (not shown).

The XRD patterns of the deposits in the 39–55° 2θ range are presented in Fig. 4. All the films are nanocrystalline or partially amorphous. The crystalline fractions belong to the hexagonal close-packed (hcp) structure. A clear evolution from a nanocrystalline towards an amorphous structure is observed with j under DC deposition conditions (Fig. 4a). This can be explained on the basis of an increasingly faster deposition rate, enhanced hydrogen coevolution and the incorporation of larger amounts of Re in the Co–Ni lattice. Deposits remain mostly crystalline in PP and RPP conditions (except for the film obtained at $j_c = -250$ mA cm^{-2} by RPP, which shows an amorphous background). Hence, another advantage of using PP and RPP methods is that Re-rich deposits (18–25 at% Re) with a nanocrystalline character can be obtained whereas those of similar composition produced by DC are mainly amorphous. Moreover, most of the films show a strong texture either on the hcp (1 0 0) or (0 0 2) planes since the $I^{1/2}(1\,0\,0)/I^{1/2}(0\,0\,2)$ intensity ratios significantly differ from the theoretical value (1.22). The texture on the (1 0 0) plane typically appears at low current densities (j and j_{on} of -50 mA cm^{-2}) while the preferred orientation on (0 0 2) planes develops at higher currents. Table 3 lists the $I^{1/2}(1\,0\,0)/I^{1/2}(0\,0\,2)$ ratios and the values of average crystallite size and microstrains, estimated from the Rietveld refinements. The crystallite size values fall within the nanometric regime (<65 nm for all deposition conditions) and are typically lower in films deposited in DC than in those deposited under PP or RPP conditions. The variations in $\langle D \rangle$ could be influenced not only by the deposition rate (higher rates would promote lower $\langle D \rangle$ values) but also by the compositions. For example, the presence of P could favour crystallite size refinement and even induce the growth of amorphous CoNiReP films, as previously observed in RPP conditions using low j_c values (e.g., -10 mA cm^{-2}) [9]. The microstrains typically increase with the applied current density for all deposition techniques while the stacking fault probability remains rather small (lower than 10^{-4} for all films). The stacking fault probability in ball-milled cobalt powders is around 10^{-1} [14], hence two orders of magnitude larger than in the electrodeposits investigated.

3.3. Mechanical and magnetic properties of the deposits

The values of nanoindentation Berkovich hardness (H_B) and the reduced Young's modulus (E_r) of the CoNiReP films are listed in Table 4. A significant variation in the mean H_B values (between 6.2 and 9.2 GPa) is observed and is influenced by a variety of factors: the electrodeposition method, the chemical composition
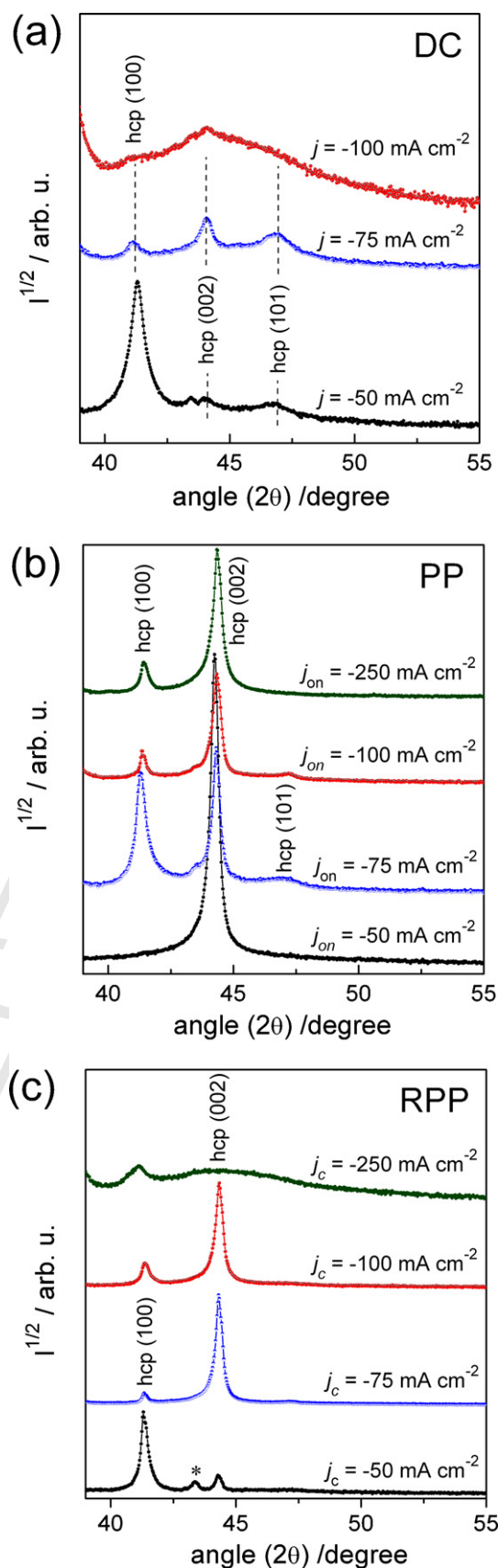
Fig. 4. XRD patterns in the 39–55° 2θ range of the CoNiReP layers obtained under (a) DC conditions as a function of the current density (j), (b) PP conditions as a function of the current density of the pulse (j_{on}), and (c) RPP conditions as a function of current density of the cathodic pulse (j_c). The peak denoted with (*) belongs to the Au seed-layer.

Table 4
Berkovich nanohardness (H_B), reduced Young's modulus (E_r), H_B/E_r, H_B^3/E_r^2 and U_e/U_t ratios for the CoNiReP films obtained by DC, PP and RPP techniques.

Technique	$-j$, $-j_{on}$ or $-j_c$/mA cm^{-2}	Composition	H_B/GPa	E_r/GPa	H_B/E_r	H_B^3/E_r^2/GPa	U_e/U_t
DC	50	$Co_{72}Ni_{17}Re_9P_1$	7.0 ± 0.1	139 ± 1	0.0505 ± 0.0002	0.0180 ± 0.0001	0.3181 ± 0.0009
	75	$Co_{65}Ni_{17}Re_{18}$	8.1 ± 0.1	160 ± 1	0.0507 ± 0.0002	0.0209 ± 0.0003	0.3140 ± 0.0007
	100	$Co_{52}Ni_{24}Re_{24}$	6.4 ± 0.1	141 ± 1	0.0450 ± 0.0003	0.0129 ± 0.0003	0.2800 ± 0.0008
PP	50	$Co_{78}Ni_9Re_9P_4$	7.1 ± 0.1	142 ± 2	0.0500 ± 0.0006	0.0177 ± 0.0015	0.2708 ± 0.0086
	75	$Co_{78}Ni_{10}Re_9P_3$	7.6 ± 0.3	159 ± 3	0.0478 ± 0.0019	0.0174 ± 0.0028	0.2807 ± 0.0067
	100	$Co_{64}Ni_{18}Re_{18}$	9.2 ± 0.3	189 ± 4	0.0487 ± 0.0020	0.0218 ± 0.0025	0.3249 ± 0.0085
	250	$Co_{34}Ni_{41}Re_{25}$	8.6 ± 0.2	168 ± 2	0.0511 ± 0.0013	0.0225 ± 0.0017	0.3414 ± 0.0013
RPP	50	$Co_{79}Ni_{10}Re_8P_3$	7.3 ± 0.1	167 ± 1	0.0437 ± 0.0007	0.0139 ± 0.0007	0.2905 ± 0.0084
	75	$Co_{76}Ni_9Re_8P_3$	8.9 ± 0.3	172 ± 2	0.0517 ± 0.0018	0.0238 ± 0.0025	0.3490 ± 0.0034
	100	$Co_{77}Ni_{11}Re_{10}P_2$	8.7 ± 0.2	165 ± 2	0.0527 ± 0.0013	0.0242 ± 0.0017	0.3620 ± 0.0062
	250	$Co_{46}Ni_{27}Re_{27}$	6.2 ± 0.1	138 ± 3	0.0449 ± 0.0012	0.0125 ± 0.0008	0.2984 ± 0.0051

and the crystallographic structure. The mechanically softest deposits correspond to the DC plated sample at $j = -100$ mA cm^{-2} (6.4 GPa) and the RPP plated sample at $j_c = -250$ mA cm^{-2} (6.2 GPa), while the hardest deposits correspond to the PP plated sample at $j_{on} = -100$ mA cm^{-2} (9.2 GPa) and the RPP plated sample at $j_c = -75$ mA cm^{-2} (8.9 GPa). The latter are ferromagnetic, as it will be shown later, whereas previous CoNiReP deposits showing similar values of hardness were virtually nonmagnetic [9]. The incorporation of Re into the deposits causes the expected increase in hardness provided that the Ni/Co ratio does not rise above ∼0.3. For example, H_B increases from 7.0 GPa for the film obtained by DC at -50 mA cm^{-2} ($Co_{72}Ni_{17}Re_9P_1$) to 8.1 GPa for the film obtained by DC at -75 mA cm^{-2} ($Co_{65}Ni_{17}Re_{18}$). Here, part of the Co has been formally replaced by Re which has much larger hardness than that of Co (hardness for bulk Re is 2.6–7.5 GPa [11]). However, further increase in the Re content promotes a concurrent increase in the amount of Ni (i.e., DC plated sample at -100 mA cm^{-2}). Taking into account the bulk hardness of Co (1.04 GPa) and Ni (0.638 GPa) [24], the increase in hardness supplied by Re is probably being mitigated by the incorporation of Ni (i.e., solid solution hardening and softening effects are counterbalanced). Also, the expected increase in hardness is not accomplished by the concomitant amorphization. Indeed, amorphous metallic alloys usually exhibit higher strength than their crystalline counterparts, because plastic deformation mechanisms driven by dislocations motion, twinning or grain boundary sliding do not operate in that case due to the lack of long-range crystallographic order [25]. Consequently, plastic deformation in amorphous metallic alloys occurs via propagation of shear bands, which require relatively high energy to nucleate, thus enhancing the material strength. The increase in surface roughness at higher applied current densities (Fig. 3) and the presence of surface porosity could contribute to reduce H_B. Regarding the PP samples, an increase in hardness with the Re content is also observed (cf. samples deposited at $j_{on} = -75$ mA cm^{-2}

and -100 mA cm^{-2} in Table 3) and again a decrease is found at $j_{on} = -250$ mA cm^{-2}. The RPP electrodeposits show similar values of hardness between -75 and -100 mA cm^{-2} due to a similar composition and crystalline nature. These results suggest that a complete understanding of the mechanical behaviour for these samples can only be understood by taking into account the interplay between different factors (composition, crystallite size, texture, etc.).

The reduced Young's modulus varies between 138 and 189 GPa. The values seem to be affected by both the composition and the microstructure (crystalline/amorphous). An increase in E_r with the Re content is usually observed, a result that one would expect considering that Re exhibits the third largest elastic modulus amongst all metals (470 GPa) [10]. However, a decrease in E_r due to amorphization of the deposits at high current density (DC at -100 mA cm^{-2} or RPP at -250 mA cm^{-2}) is also seen. Such a decrease is probably related to the existence of free volume in the amorphous structure and the occurrence of anharmonic vibrations resulting from the chemical and topological disorder of the glassy metallic alloys, thus causing elastic softening [10,26]. A similar effect is also seen if one compares the DC sample at -75 mA cm^{-2} with the PP sample at $j_{on} = -100$ mA cm^{-2}. Their composition is almost identical but E_r of the latter is significantly higher (189 GPa versus 160 GPa). The DC sample has a significant amorphous background whereas the PP sample is crystalline.

Table 4 also lists the values of H_B/E_r, H_B^3/E_r^2 and U_e/U_t ratios, where U_e is the elastic energy and U_t the total (elastic + plastic) energy. The values of U_e and U_t were estimated from the areas enclosed between the unloading indentation segment and the displacement axis (U_e) and between the loading segment and the displacement axis (U_t). The ratio of hardness to reduced modulus (H_B/E_r) provides an indirect assessment of the wear resistance of a coating [27]. For most of the films, the H_B/E_r ratio is about 0.05. The highest values are obtained in CoNiReP films with high Re content that preserve a nanocrystalline (i.e., not amorphous)

Table 5
Coercivity (H_C) (parallel and perpendicular to the film plane), saturation magnetization (M_S) and remanence-to-saturation ratios (M_R/M_S) (parallel and perpendicular to the film plane) for the CoNiReP films obtained by DC, PP and RPP techniques. Correction for the demagnetizing field was applied [17–19]. The error in H_C and M_S are within ±5 Oe and 5%, respectively.

Technique	$-j$, $-j_{on}$ or $-j_c$/mA cm^{-2}	Composition	$H_{C\parallel}$/Oe	$H_{C\perp}$/Oe	M_S/emu cm^{-3}	$M_R/M_{S\parallel}$	$M_R/M_{S\perp}$
DC	50	$Co_{72}Ni_{17}Re_9P_1$	735	2265	538	0.56	0.53
	75	$Co_{65}Ni_{17}Re_{18}$	107	223	398	0.39	0.14
	100	$Co_{52}Ni_{24}Re_{24}$	33	60	221	0.17	0.05
PP	50	$Co_{78}Ni_9Re_9P_4$	1018	1390	772	0.31	0.24
	75	$Co_{78}Ni_{10}Re_9P_3$	728	1080	730	0.41	0.34
	100	$Co_{64}Ni_{18}Re_{18}$	441	1033	376	0.35	0.15
	250	$Co_{34}Ni_{41}Re_{25}$	710	1470	550	0.32	0.23
RPP	50	$Co_{79}Ni_{10}Re_8P_3$	540	2607	758	0.48	0.70
	75	$Co_{76}Ni_9Re_8P_3$	740	950	732	0.43	0.30
	100	$Co_{77}Ni_{11}Re_{10}P_2$	883	1532	711	0.46	0.24
	250	$Co_{46}Ni_{27}Re_{27}$	<2	60	53	0.04	0.05
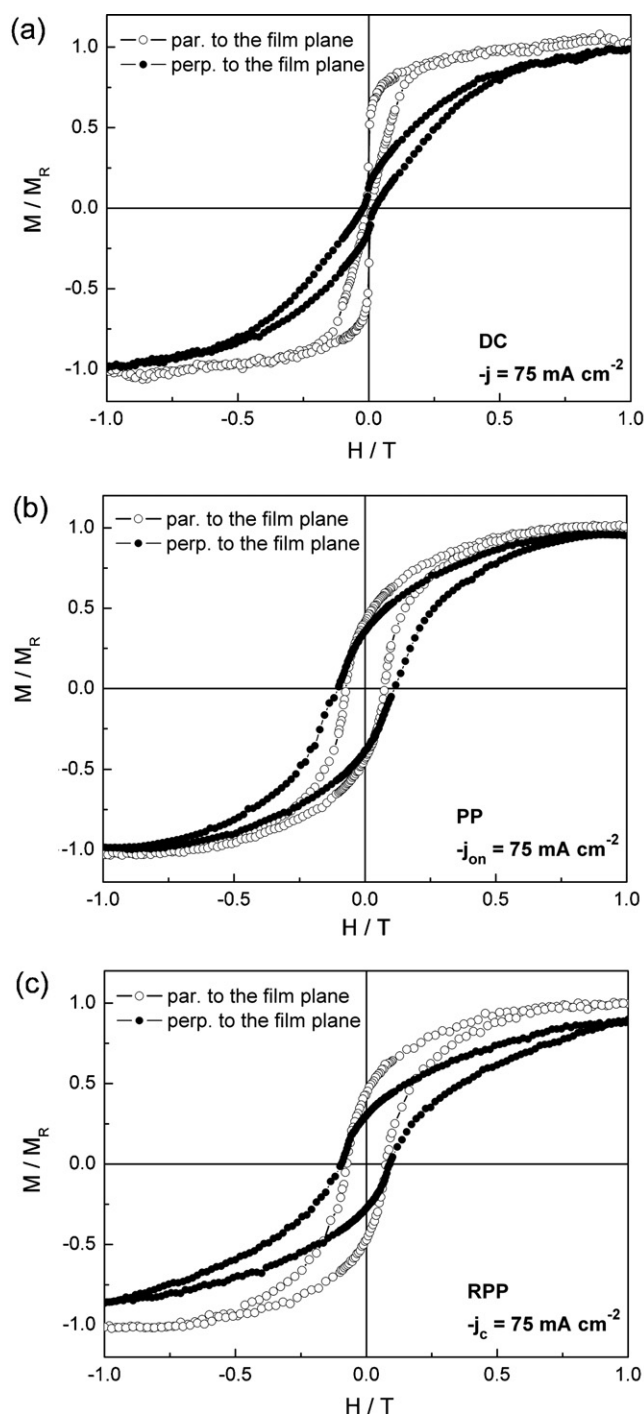
Fig. 5. Room temperature hysteresis loops measured parallel and perpendicular to the film plane for the deposits obtained in DC, PP and RPP conditions at −75 mA cm^{-2} (j, j_{on} and j_c, respectively).

microstructure. The resistance to plastic deformation (H_B^3/E_r^2) follows the same trend as the H_B/E_r values. Finally, the elastic recovery (U_e/U_t), which is a parameter of particular interest in applications such as impact loading (since it indicates how much energy is released from the material after being loaded), ranges between 0.27 and 0.36. Again, enrichment in Re typically causes an increase of U_e/U_t, provided that the films remain nanocrystalline. This is not surprising, bearing in mind that the U_e/U_t ratio is often correlated with H_B/E_r [28]. In Re-rich nanocrystalline films the values surpass those of nanocrystalline Cu–Ni [29] or Co–Ni [28] deposits, measured using the same set-up and similar conditions.

Concerning the magnetic properties, the deposits range from soft to semi-hard ferromagnetic depending on the preparation conditions (see Fig. 5). In a first approximation, the saturation magnetization (M_S) increases with the Co content (Table 5) with the exception of the Ni-rich sample prepared under PP conditions at $j_{on} = -250$ mA cm^{-2}. The increase of M_S with the Co content is to be expected since $M_{S,Ni} = 490$ emu cm^{-3} is much lower than that of Co ($M_{S,Co} = 1425$ emu cm^{-3}). In the case of electroless-deposited CoNiReP films, M_S has been reported to depend not only on the Co content but also on the crystalline fraction, i.e., lower crystalline films tend to be non-ferromagnetic [3]. In DC and RPP conditions, the increase in Ni content is correlated with an increase in amorphicity, but this is not the case in the PP sample prepared using $j_{on} = -250$ mA cm^{-2}. Therefore, the moderate M_S value observed in this film could be related to the lack of amorphicity despite its large Ni content.

Similar to what had been observed for DC and RPP films deposited at low current densities (≤ -50 mA cm^{-2}) [9], the coercivity (H_C) for all samples is larger along the perpendicular-to-film direction than along the in-plane direction. However, in most cases the remanence-to-saturation ratio, M_R/M_S, is larger along the in-plane direction and the loops are more sheared along the perpendicular-to-plane direction, indicating the predominant role of shape anisotropy, which favours in-plane magnetic easy axis behaviour. This is opposite to what had been observed in some of the CoNiReP alloys electrodeposited at low current densities [9], where perpendicular-to-film effective magnetic anisotropy was observed and ascribed to the presence of moderate amounts of P and Re in their composition. The current investigation suggests that the magnetic anisotropy direction critically depends on the alloy composition. A large amount of Re, combined with lack of P, is not favourable to induce perpendicular-to-film magnetic easy axis, which would be desirable in applications such as perpendicular recording media or out-of-plane magnetic actuators. The coercivity of amorphous-like CoNiReP films is lower than for crystalline ones, both along in-plane and perpendicular-to-plane directions. The H_C value not only depends on the composition and the degree of crystallinity, but could also depend on the crystallographic texture. Consequently, the interpretation of the H_C dependence on the applied current density (Table 5) is not straightforwardly correlated. In any case, most of the Co-rich CoNiReP alloys prepared using relatively low applied current densities (from −10 to −50 mA cm^{-2}) were magnetically harder (i.e., with larger H_C values, particularly along the perpendicular direction) than the ones presented here [9]. This indicates that exceedingly large Re contents cause the electrodeposited films to be magnetically softer, probably due to the reduction of Co content and higher amorphization. The obtained films could be applied in mobile magnetic components where soft-magnetic response combined with mechanical stability under contact and friction is required (e.g., magnetic bearings).

4. Conclusions

A systematic study of the composition, structure, mechanical properties, and magnetic behaviour of CoNiReP films has been conducted as a function of the electrodeposition technique (DC, PP and RPP) in the range of cathodic current densities from −50 mA cm^{-2} to −250 mA cm^{-2}. Co-rich, P-containing deposits are obtained at values of j (DC), j_{on} (PP) and j_c (RPP) below −100 mA cm^{-2}. Further increase of the current density significantly promotes the incorporation of Re into the deposits while the P content virtually falls to zero. It is demonstrated that adherent, nanocrystalline CoNiReP alloy films with Re contents up to 25 at%, not previously achieved by electroless deposition, can be obtained by PP at $j_c = -250$ mA cm^{-2}. Under DC conditions, deposits tend to peel from the substrate at

current densities higher than −100 mA cm^{-2} and amorphization of the deposits is unavoidable. Deposits that combine large hardness values (8.9–9.2 GPa) and pronounced elastic recovery with ferromagnetic behaviour have been obtained by both PP and RPP depositions. These deposits could be useful in mobile magnetic devices where soft or semi-hard magnetic components are required to operate under contact or friction.

Acknowledgements

References

[1] T. Osaka, I. Koiwa, M. Toda, T. Sakuma, Y. Yamazaki, T. Namikawa, F. Goto, IEEE Transactions on Magnetics 22 (1986) 1149.

[2] H. Matsubara, H. Mizutani, S. Mitamura, T. Osaka, F. Goto, IEEE Transactions on Magnetics 24 (1988) 3018.

[3] T. Osaka, H. Matsubara, M. Toda, T. Homma, Journal of the Electrochemical Society 136 (1989) 2637.

[4] T. Osaka, T. Homma, K. Inoue, Y. Yamazaki, T. Namikawa, IEEE Transactions on Magnetics 5 (1990) 154.

[5] T. Homma, T. Osaka, Journal of the Electrochemical Society 139 (1992) 2925.

[6] T. Homma, K. Sato, T. Osaka, Japanese Journal of Applied Physics 29 (1990) 1701.

[7] E. Valova, S. Armyanov, J. Dille, Y. Van Ingelgem, A. Hubin, O. Steenhaut, Journal of the Electrochemical Society 155 (2008) D449.

[8] W.B. Ng, A. Takada, K. Okada, IEEE Transactions on Magnetics 41 (2005) 3886.

[9] S. Pané, E. Pellicer, K.M. Sivaraman, S. Suriñach, M.D. Baró, B.J. Nelson, J. Sort, Electrochimica Acta 56 (2011) 8979.

[10] A. Naor, N. Eliaz, E. Gileadi, Electrochimica Acta 54 (2009) 6028.

[11] A. Naor, N. Eliaz, E. Gileadi, S.R. Taylor, The AMMTIAC Quarterly 5 (2010) 11.

[12] J.Cl. Puippe, Plating and Surface Finishing 67 (1980) 68.

[13] L. Lutterotti, S. Gialanella, Acta Materialia 46 (1998) 101.

[14] J. Sort, J. Nogués, S. Suriñach, M.D. Baró, Philosophical Magazine 83 (2003) 439.

[15] A.C. Fischer-Cripps, in: F.F. Ling (Ed.), Nanoindentation, Springer, New York, 2004.

[16] W.C. Oliver, G.M. Pharr, Journal of Materials Research 7 (1992) 1564.

[17] U. Admon, M.P. Dariel, E. Grunbaum, J.C. Lodder, Journal of Applied Physics 62 (1987) 1943.

[18] P.L. Cavallotti, M. Bestetti, S. Franz, Electrochimica Acta 48 (2003) 3013.

[19] J. Wu, L. Holloway, H. Laidler, K. O'Grady, S. Khizroev, J.K. Howard, R.W. Gustafson, D. Litvinov, IEEE Transactions on Magnetics 38 (2002) 1682.

[20] M.S. Chandrasekar, M. Pushpavanam, Electrochimica Acta 53 (2008) 3313.

[21] E. Valova, S. Armyanov, A. Franquet, A. Hubin, O. Steenhault, J.-L. Delplancke, J. Vereecken, Journal of Applied Electrochemistry 31 (2001) 1367.

[22] D. Mencer, Journal of Alloys and Compounds 306 (2000) 158.

[23] F. Pearlstein, R.F. Weightman, Plating 54 (1967) 714.

[24] http://webelements.com

[25] A. Concustell, J. Sort, G. Alcalá, S. Mato, A. Gebert, J. Eckert, M.D. Baró, Journal of Materials Research 20 (2005) 2719.

[26] J. Fornell, S. Suriñach, M.D. Baró, J. Sort, Intermetallics 17 (2009) 1090.

[27] A. Leyland, A. Matthews, Wear 246 (2000) 1.

[28] E. Pellicer, S. Pané, K.M. Sivaraman, O. Ergeneman, S. Suriñach, M.D. Baró, B.J. Nelson, J. Sort, Materials Chemistry and Physics 130 (2011) 1380.

[29] E. Pellicer, A. Varea, S. Pané, B.J. Nelson, E. Menéndez, M. Estrader, S. Suriñach, M.D. Baró, J. Nogués, J. Sort, Advanced Functional Materials 20 (2010) 283.